Soft Matter

Accepted Manuscript

This article can be cited before page numbers have been issued, to do this please use: O. F. Aguilar Gutierrez and A. D. Rey, *Soft Matter*, 2018, DOI: 10.1039/C7SM02409F.

ROYAL SOCIETY OF CHEMISTRY

rsc.li/soft-matter-journal

View Article Online
DOI: 10.1039/C7SM02409F

Extracting Shape from Curvature Evolution in Moving Surfaces

Oscar F. Aguilar Gutierrez[a] and Alejandro D. Rey[a]*

[a]*Department of Chemical Engineering, McGill University*
Montreal, Quebec, Canada H3A 0C5
**Corresponding author: alejandro.rey@mcgill.ca*

Abstract

Shape is a crucial geometric property of surfaces, interfaces, and membranes in biology, colloidal and interface science, and many areas of physics. This paper presents theory, simulation and scaling of local shape and curvedness changes in moving surfaces and interfaces, under uniform normal motion, as in phase ordering transitions in liquid crystals. Previously presented measures of shape and curvedness are introduced in quantities and equations used in colloidal science and interfacial transport phenomena to separate shape effects from those of curvedness. Considering in parallel the new shape formalism with the classical curvature formalism, this paper sheds new light on what effects originate only from shape. The new shape evolution equations are solved under uniform normal surface flow. It is found that the solutions obey the so-called "astigmatism equation" fixing the linear relation between the radii of curvature. Astigmatic trajectories in the shape-curvedness phase plane, can be clearly classified into two modes: (i) constant shape evolution, and (ii) variable shape-variable curvedness. Shapes between spheres and cylinders follow the former mode for large curvedness and transition at smaller curvedness into the latter. Shapes transitions between cylinder and saddles only follow the second mode. Under geometry-driven stagnation (i.e. zero normal velocity) shapes can be frozen. Evolving spheres and cylinders freeze into the same original shape, but perturbed cylinders can freeze into a variety of shapes including saddles.

View Article Online
DOI: 10.1039/C7SM02409F

The results provide a useful complementary view on how to describe and control shape evolution in surfaces and interfaces, of wide interest in soft matter materials.

1. Introduction

The separation of shape and size is well established in the physics of particle-fluid suspensions, matrix-filler composites and other multi-phase media [1-3]. The effects on such separation in mechanical properties, such as viscosity in suspensions and moduli in composites [1-3] is of great relevance to design of material systems and processes. In these examples shapes are introduced with the use of a shape parameter and/or sphericity index while size is introduced using various equivalent diameters, according to applications. These indexes have been successful due to accurate predictability.

In interfacial transport phenomena and related fields [4], shape is usually identified using various scalar curvature measures, such as the Gaussian and the mean curvature. With these scalar measures one can classify shapes such as saddles, cylinders, and spheres [4,5]. On the other hand, it has been shown [6] that curvatures do not separate intrinsic shape from the degree of curvedness, such as when comparing large and small spheres or large and small cylinders. In a large range of fields, such as visual recognition [7,8], morphogenesis in biology [9], phase transitions in metals [11], a separation of shape and curvedness has been implemented and shown to be a very useful approach when these two independent quantities need to be established. For example, in biological studies cylindrical bacterial growth through constant shape and curvedness, offers crucial advantages such as in cell division [10]. Control and optimization of fluid-solid interactions to minimize friction drag is another well-known area were shape determination is of great relevance.

View Article Online
DOI: 10.1039/C7SM02409F

Having established the importance and need to distinguish shape from curvedness we next quantify these ideas by introducing the shape-curvedness space [6], shown in Figure 1. This 2D space specify the shape (x-axis, dimensionless) , such as cylinder, saddle or sphere and the curvedness (y-axis, with units of reciprocal length L^{-1}) which is an indication of non-flatness [6]. Fig. 1 shows three characteristic trajectories that specify the modes of temporal evolution under motion: (i) shape invariant evolution (vertical line), (ii) constant curvedness evolution (horizontal line), (iii) variable shape-variable curvedness evolution (arbitrary curve). In this paper we seek to find the specific conditions that lead to evolution under constant shape, such as growing cylinders and those conditions leading to shape changes, such as a quasi-cylinder becoming a saddle. In this paper we only consider non-material local surface patches that exist between two bulk phases, such as the nematic-isotropic interface during the order-disorder transition. It is worth noting global shape evolution is outside the scope of this paper, but our description could be applied locally to these cases.

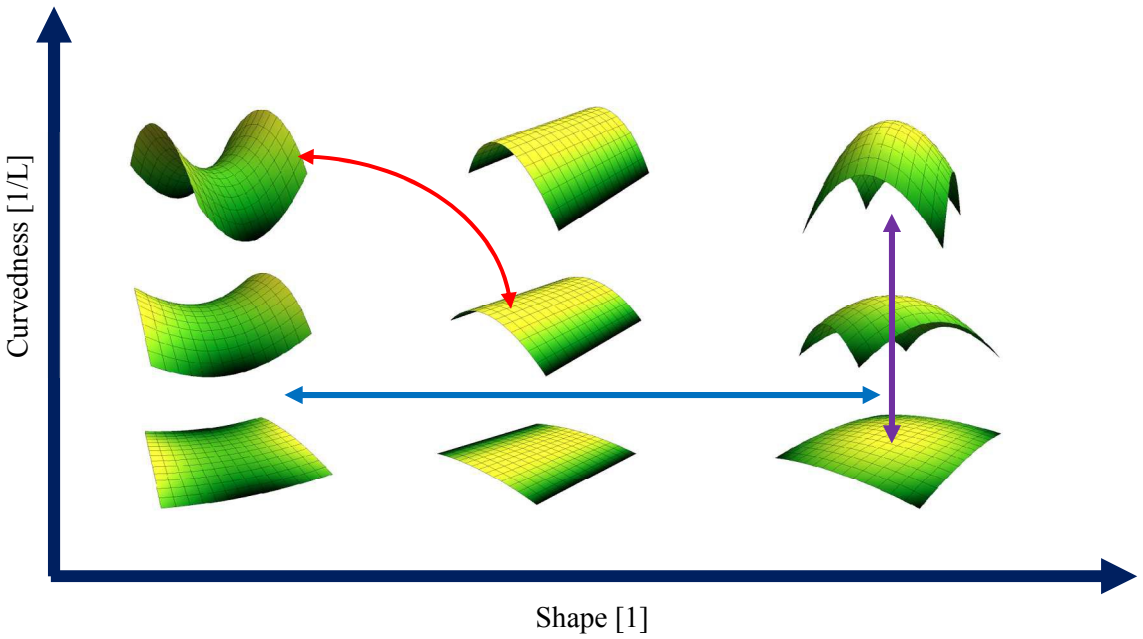

View Article Online
DOI: 10.1039/C7SM02409F

Figure 1. Curvedness-Shape space for surface patches. Evolution of surface patches can be at constant shape (vertical purple line), constant curvedness (horizontal blue line), or variable shape-variable curvedness (curved red line). Under the well-known and frequent normal uniform motion, the first or the last mode are possible.

Given the importance of decoupling shape from curvedness, in this paper we introduce shape and curvedness quantities and incorporate them in the evolution of surfaces and interfaces, restricting the surface patch motion to that of uniform normal motion. The case of uniform normal motion was previously introduced by [12,13] to analyze metal solidification and is the appropriate starting point in this new formulation to the kinetics of interfacial shaping. In uniform normal motion only, the uniform normal interface velocity is taken into account and no spatial gradients are present [12]. The purely normal velocity is accommodated by selecting a moving coordinate system in which tangential velocity is zero [14], which is a good choice for non-material surfaces. The shape-curvedness approach used in this paper was further extended with great impact in hard materials; see for example [15]. Here we extend this shape-curvedness approach to soft matter materials undergoing phase ordering transitions under uniform normal motion, where the normal velocity V is given by a balance of thermodynamic/elastic driving forces $\mathcal{L}$ and capillary pressure p_c [16-20]:

$$\beta V = \mathcal{L} + p_c \qquad (1)$$

where β is a viscosity coefficient.

Next we describe the objectives and scope of this work. The paper compares the traditional curvature approach (mean and Gaussian curvature) with the decoupled shape-curvedness approach. A few well-known examples from soft matter are firstly re-described with the shape-curvedness approach, with the objective of establishing correspondence and complementarity. Then we consider temporal surface evolution under uniform motion and show that it leads to the "astigmatism equation", which emerges when there is a linear

View Article Online
DOI: 10.1039/C7SM02409F

relation between the two surface main radii of curvature. When the found astigmatic evolution is converted into shape-curvedness evolution, we then clearly identify conditions that lead to shape-invariant evolution such as in cylindrical and spherical patches and those that lead to saddles. Finally, we take into account stagnation, that is conditions where V in eqn. (1) vanishes [21], freezing the evolving shape into characteristic shape-curvature families. In particular, we find that the cylindrical shape can evolve and freeze into low curvedness spherical patches, intermediate curvedness cylindrical patches, or high curvedness saddles and vice versa. On the other hand, spherical patches always retain their shape and stagnation just freezes the curvedness.

The organization of this paper is as follows. Section 2 treats the geometric characterization of surfaces using the well-known curvature approach and it introduces the shape-curvedness properties, previously presented in [6]. Examples of the shape-curvedness method to surfactant packing and capillary pressure establish how shape enters into these phenomena. Section 3 presents geometric evolution under uniform normal surface motion using first the curvature approach and then the new shape-curvedness method. We show how this important motion leads to an evolution according to the "astigmatic equation". We also show how the perturbed cylindrical shape can evolve into spherical, cylindrical or saddle patches. As mentioned above we only consider local surface patches, uniform normal motion. Global aspects, closed surfaces, velocity gradients, changes in the metric are not in the scope of this paper.

2. Geometric Characterization of Surfaces: Curvatures, Shape and Curvedness

The surface geometry is characterized by the symmetric 2x2 curvature tensor **b** [4]:

$$\mathbf{b} = -\nabla_s \mathbf{k} \quad = \kappa_1 \mathbf{e}_1\mathbf{e}_1 + \kappa_2 \mathbf{e}_2\mathbf{e}_2 \tag{2}$$

View Article Online
DOI: 10.1039/C7SM02409F

where $\{\kappa_m, \mathbf{e}_m\}$, m = 1, 2 are the eigenvalues and eigenvectors of $\mathbf{b}$, $\nabla_s = \mathbf{I}_s \cdot \nabla$ is the interfacial gradient operator, $\mathbf{I}_s = \mathbf{I} - \mathbf{kk}$ is the surface unit dyadic, $\mathbf{k}$ is the surface unit normal, and ∇ is the 3D gradient operator. The principal curvatures κ_1, κ_2 (eigenvalues of $\mathbf{b}$) define the principal radii of curvature (R_m) of the surface: $\kappa_m = -1/R_m$. The curvature tensor $\mathbf{b}$ can be decomposed into a trace $H\mathbf{I}_s$ and a deviatoric $D\mathbf{q}$ curvature tensor [22-25] as express in:

$$\mathbf{b} = H\mathbf{I}_s + D\mathbf{q};\ 2H = \kappa_1 + \kappa_2;\ 2D = \kappa_1 - \kappa_2 \qquad (3)$$

The reader is referred to Appendix A for the mathematical detail. The magnitude of the deviatoric curvature D is a useful non-sphericity index since it vanished for a sphere (D = 0); without loss of generality we use D>0. Defining the deviatoric curvature tensor $\mathbf{f} = H\mathbf{I}_s - \mathbf{b} = -D\mathbf{q}$, we find by using $\mathbf{b}$ and $\mathbf{f}$, the mean H, Gaussian K, square deviatoric D^2, and Casorati C curvatures [6,26] as follows:

$$H = \frac{1}{2}\boldsymbol{\varepsilon}_s : \left(\mathbf{I}_s \cdot \boldsymbol{\varepsilon}_s \cdot \mathbf{b}\right); K = \frac{1}{2}\boldsymbol{\varepsilon}_s : \left(\mathbf{b} \cdot \boldsymbol{\varepsilon}_s \cdot \mathbf{b}\right); D^2 = \frac{1}{2}\mathbf{I}_s : \left(\mathbf{f} \cdot \mathbf{I}_s \cdot \mathbf{f}\right); C^2 = \frac{1}{2}\mathbf{I}_s : \left(\mathbf{b} \cdot \mathbf{I}_s \cdot \mathbf{b}\right) \qquad (4)$$

where $\boldsymbol{\varepsilon}_s = -\mathbf{k} \times \mathbf{I}_s$ is the surface alternator dyadic. These curvatures are summarized on Table 1.

View Article Online
DOI: 10.1039/C7SM02409F

Table 1. Four curvatures based on the curvature tensor **b** and deviatoric curvature tensor **f**.

Curvatures	Symbols	Relations	Tensor Contractions	Principal Curvatures
Mean	H	H	$\boldsymbol{\varepsilon}_s : \left(\mathbf{I}_s \cdot \boldsymbol{\varepsilon}_s \cdot \mathbf{b}\right)/2$	$\frac{\kappa_1 + \kappa_2}{2}$
Gaussian	K	K	$\boldsymbol{\varepsilon}_s : \left(\mathbf{b} \cdot \boldsymbol{\varepsilon}_s \cdot \mathbf{b}\right)/2$	$\kappa_1 \kappa_2$
Deviatoric	D	$\sqrt{H^2\text{-}K}$	$\sqrt{\mathbf{I}_s : \left(\mathbf{f} \cdot \mathbf{I}_s \cdot \mathbf{f}\right)/2}$	$\frac{\kappa_1 - \kappa_2}{2}$
Casorati	C	$\sqrt{H^2+D^2}$	$\sqrt{\mathbf{I}_s : \left(\mathbf{b} \cdot \mathbf{I}_s \cdot \mathbf{b}\right)/2}$	$\sqrt{\frac{\kappa_1^2 + \kappa_2^2}{2}}$

The usual surface patch shape characterization is based on the HK or equivalently HD curvatures, shown in Table 2.

Table 2. Surface shape classification according to the HK(HD) method.

Surface Patch	Curvatures
cylinder (ridge,rut)	H=D;H=-D, K=0
spherical cap	D=0, K>0
saddle	H=0, K<0

H: mean; D: deviatoric, K: Gaussian curvatures

View Article Online
DOI: 10.1039/C7SM02409F

In this HK characterization, the intrinsic surface shape and the magnitude of curvedness are co-mingled since these curvatures are not dimensionless. To decouple these two quantities, the shape-curvedness (SC) classification was proposed [6], which uses Casorati's C curvature (see Table 1) and a normalized function of the ratio H/D:

$$S = \frac{2}{\pi}\tan^{-1}\left(\frac{H}{|D|}\right) \quad (5)$$

The shape index ($-1 < S \leq +1$) gives a continuous evolution between shapes, with S = 0 denoting a saddle, S = 1/2 a cylinder and S = 1 a sphere; for a surface patch the sign of S defines the concavity, with S = +1/2 the cylindrical patch is concave up and for S = -1/2 concave down. The SC classification corresponding to Table 2 is shown in Figure 2, adapted from [7].

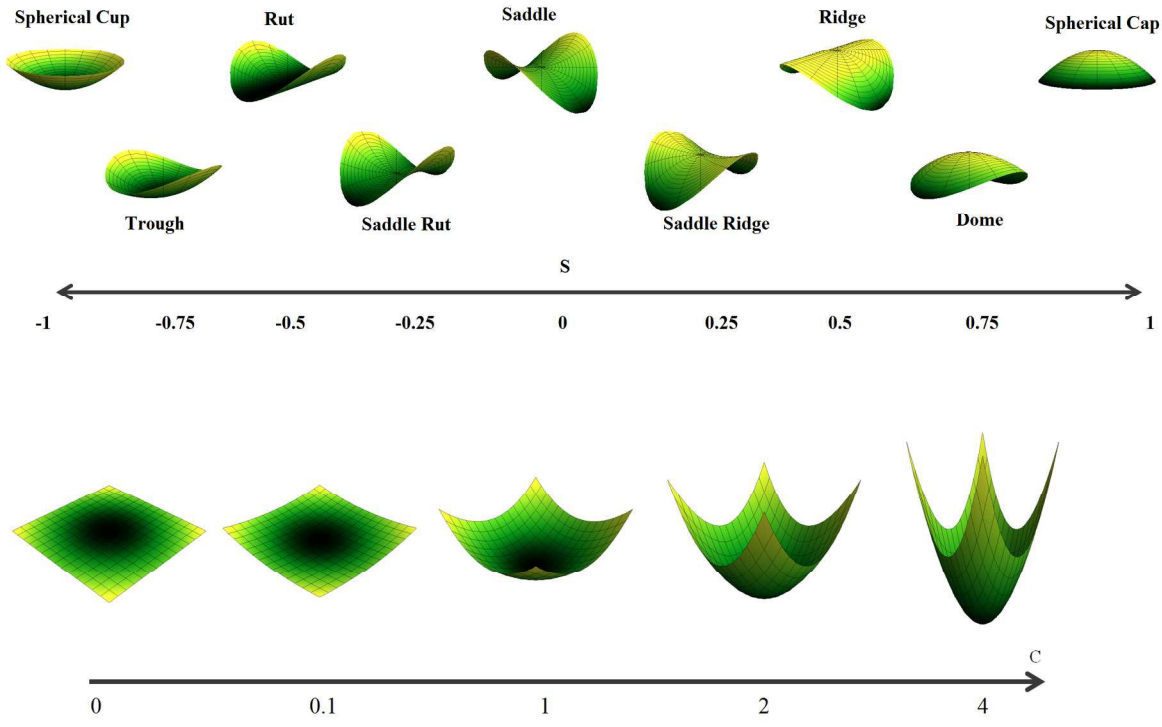

View Article Online
DOI: 10.1039/C7SM02409F

Figure 2. (a) Classes in shape space; adapted from [7]. (b) Curvedness space for a constant shape, showing changes in Casorati's C curvature.

Expressing $\{H, D\}$ in terms of $\{S, C\}$, shows that the HD scheme comingles shape S and curvedness C :

$$H = C\sin\left(\frac{S\pi}{2}\right);\quad |D| = C\cos\left(\frac{S\pi}{2}\right); K = -C^2\cos(S\pi) \tag{6}$$

In this convention H<0 (H>0), when -1<S<0 (0<S<1), and D>0 for -1<S<1. If we consider the transformation between the HD and SC systems, we find:

$$\begin{bmatrix} dH \\ dD \end{bmatrix} = \begin{bmatrix} \sin\left(\frac{S\pi}{2}\right) & \frac{\pi}{2}C\cos\left(\frac{S\pi}{2}\right) \\ \cos\left(\frac{S\pi}{2}\right) & -\frac{\pi}{2}C\sin\left(\frac{S\pi}{2}\right) \end{bmatrix} \begin{bmatrix} dS \\ dC \end{bmatrix} \tag{7}$$

then it follows that when HD are fixed (dH=dD=0) then SC are also fixed (dC=dS=0) , but if only H is fixed then only a function S=f(C) if fixed and in principle different shapes with different curvedness can meet the H-constraints. Some representative examples of the SC approach based on soft matter models follow.

2.1 Statics

(i) Shape equation for anisotropic surfaces

In the statics of surfaces and interfaces the shape equation is [16-20]:

$$-|\mathbf{T}:\mathbf{kk}| = -2\left(\gamma + \mathbf{I}_s : \frac{\partial^2\gamma}{\partial\mathbf{k}^2}\right)H = bC\sin\left(\frac{S\pi}{2}\right) \tag{8}$$

where $\gamma(\mathbf{k})$ is the interfacial tension, $|\mathbf{T}:\mathbf{kk}|$ is the bulk stress load,

View Article Online
DOI: 10.1039/C7SM02409F

$\mathbf{I}_s : \partial^2\gamma / \partial \mathbf{k}^2$ is the Herring's pressure [17,18] and $b = 2\left(\gamma + \mathbf{I}_s : \partial^2\gamma / \partial \mathbf{k}^2\right)$ is the anisotropic tension; more general equations that include director orientation are not discussed for brevity. We note that the shape equation (8) contains the Casorati curvature as well. Defining $\left|\mathbf{T} : \mathbf{kk}\right| \equiv a$, we find that solutions to the shape equation (8) are grouped into three characteristic SC static modes:

(i)no load, flat surface : $a = 0, C = 0$
(ii)no load, saddle surface : $a = 0, S = 0$
(iii)load, curved shapes: $C\sin\left(S\pi / 2\right) = \Lambda$

where the constant Λ=-a/b. As shown in Fig. 3, these three modes in the statics of surfaces and interfaces are the main axes of the CS plane and hyperbola-like trajectories.

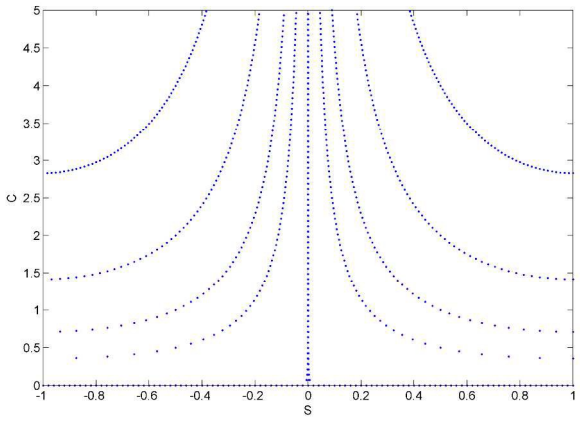

Figure 3. Three possible shape-curvedness modes: (i) flat surface (C = 0), (ii) saddle surface (S = 0) and (iii) arbitrary shapes $\left(C\sin\left(S\pi / 2\right) = \Lambda = \text{const}, C > 0, 0 < |S| \le 1\right)$.

The SC approach gives a compact representation to the solutions of the anisotropic shape equation (8).

(ii) Surfactant self-assembly and parallel surfaces

View Article Online
DOI: 10.1039/C7SM02409F

In a family of parallel surfaces schematically depicted in figure 4a, the relationship between the area A_o on the parent surface and area $A(\lambda)$ at a distance λ from the parent surface is given by [14]:

$$h = \frac{A(\lambda)}{A_o} = 1 - 2H\lambda + K\lambda^2 = (1-\lambda\kappa_1)(1-\lambda\kappa_2) \quad >0 \tag{9}$$

where h is the area magnification factor. In surfactant self-assembly h is fixed by the surfactant self-assembly process [5]. Integrating the area magnification factor h with respect to λ from 0 to ℓ (surfactant molecule length), and dividing by ℓ one finds the surfactant packing factor f (S,C):

$$f = 1 - (\ell\, C)\sin\left(\frac{S\pi}{2}\right) - \frac{(\ell C)^2}{3}\cos(S\pi)$$

$$\ell\, C = \frac{-\sin(S\pi/2) + \sqrt{\sin^2(S\pi/2) + 4(1-f)\cos(S\pi)/3}}{2\cos(S\pi)/3} \tag{10 a-b}$$

Fixing f=1/3,1/2,1, one finds three characteristic SC pairs:

(i)planes : $f = 1; C = 0$

(ii)spheres : $f = \frac{1}{3}; S = 1; \ell C = 1$

(iii)cylinder : $f = \frac{1}{2}; S = 1/2; \ell C = \frac{1}{\sqrt{2}}$

These results agree with the standard surfactant packing model and show how pure shape S and curvedness C adapt to the surfactant factor f ,as shown in figure 4b.

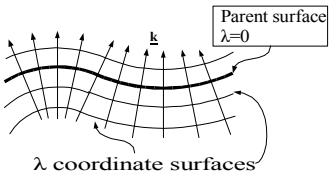

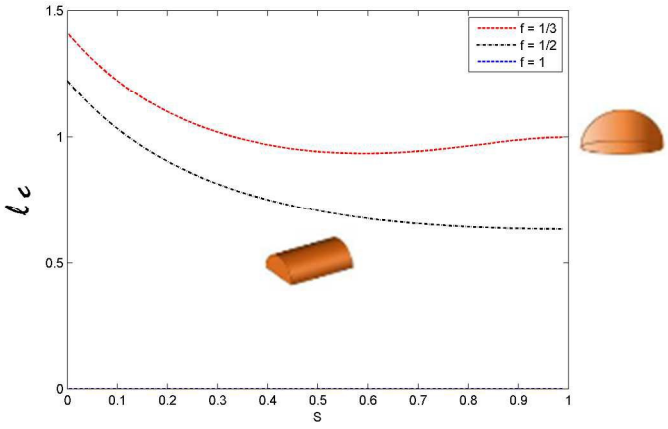

View Article Online
DOI: 10.1039/C7SM02409F

Figure 4. Parallel surfaces (a) and effect of packing parameter constraint (b) in the SC description.

2.2 Kinematics

In addition to statics,c SC descriptions also are found for kinematics and shape evolution of surfaces and interfaces. The surface normal velocity V under a phase ordering conservative phase transition (see eqn.(1)) is given by the net sum of the stress load $\left|\mathbf{T}:\mathbf{kk}\right| \equiv \mathrm{a}$ (these are thermodynamic and elastic forces) and the capillary pressure $2\left(\gamma + \mathbf{I}_s : \partial^2\gamma / \partial \mathbf{k}^2\right)\mathrm{H}$ [17,18]:

$$\beta \mathrm{V} = \left|\mathbf{T}:\mathbf{kk}\right| - 2\left(\gamma + \mathbf{I}_s : \frac{\partial^2 \gamma}{\partial \mathbf{k}^2}\right)\mathrm{H} = \mathrm{a} + \mathrm{bC}\sin\left(\frac{\mathrm{S}\pi}{2}\right) \qquad (11\ \text{a-b})$$

where the direction and magnitude of V depend on a, b, C and S; here we use the nomenclature of eqns.(6,8) . If the stress load is zero we recover the usual motion by mean curvature and if the capillary pressure is zero we recover the constant speed phase ordering transformation, as introduced in eqn.(1). Stagnation (V = 0) arises under static equilibrium given in eqn. (8) and Figure 3.One can see that in the general case, when *a* and *b* are given , stagnation if it happens, will depended on specific values $\left\{\mathrm{S}^*\mathrm{C}^*\right\}$ of shape and curvedness: $0 = \mathrm{a} + \mathrm{bC}^* \sin\left(\mathrm{S}^*\pi / 2\right)$. When surface evolution comes to a halt, a frozen shape may appear.

View Article Online
DOI: 10.1039/C7SM02409F

Returning to the general time evolving case, the two characterizing limit behaviors described by eqn. (11) are: (i) constant shape S evolution which fixes the ratio H/D to an arbitrary constant and (ii) constant curvedness C in which the sum of the squares H^2+D^2 is fixed to another arbitrary constant. These are schematically shown as circular and radial trajectories in the DH plane shown in Figure 5.

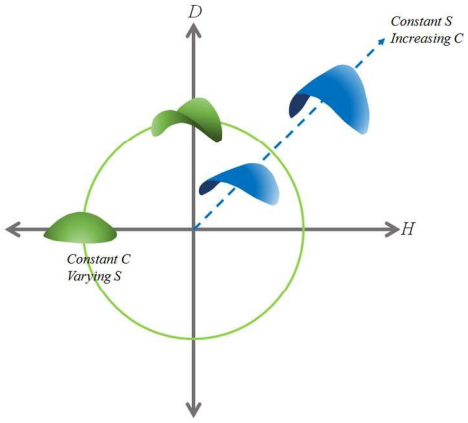

Figure 5. Shape (S)-curvedness (C) trajectories in the HD curvature space. Circular trajectories corresponds to constant C and radial trajectories to constant S. These trajectories correspond to solutions of eqn.(11).

For instance, a flat patch curving into a cap**,** we have $K = C^2$ and when curving into a saddle $K = -C^2$. Shape invariant changes retain a constant S, such as in a growing cylinder where S=1/2 but in this case the curvedness C will decrease. Hence temporal evolutions plotted in DH space can be associated with distinct degrees of shape changes.

3. Geometric Evolution under Uniform Normal Motion

In this section we describe the surface evolution under uniform normal motion, which is widely present in phase ordering transitions in soft matter systems, where the velocity vector is normal to the surface patch and constant. We first provide results for curvature evolution and then we present shape evolution.

View Article Online
DOI: 10.1039/C7SM02409F

(i) Curvature Evolution

The curvature kinematics is described [27-29]:

$$\dot{H} = \left(H^2 + D^2\right)V, \quad \dot{D} = 2HDV, \quad \dot{K} = 2HKV \qquad (12\ a\text{-}c)$$

where the sign of V is determined by eqn. (11). As shown in Appendix B the first integral for the curvatures' evolution is the relation:

$$K(t) = H^2(t) - D^2(t) = -mD(t) \qquad (13)$$

where m is a shape parameter:

$$Sphere: S = \pm 1, m \to \pm\infty; \ Cylinder: S = \pm 1/2, m = 0; Saddle: S = 0, m > 0$$

Here we consider $m \to \pm\infty$, since by definition eqn. (6) D > 0 in all cases. We note that a basically equivalent equation to (13) was derived in [12] but not in terms of D and that no connection with shape was established.

Introducing the radii of curvature ($\kappa_m = -1/R_m$) into eqn. (13) we find:

$$R_2(t) = R_1(t) + \frac{2}{m} \qquad (14)$$

which is the well-known astigmatism equation [30,31]. Using the radius of curvatures plane (R_2 versus R_1) , Figure 6 shows that for each shape m, the geometric evolution follows an astigmatism line of slope +1. For a sphere the line traverses the origin. Lines parallel to the sphere describe evolution of patches of shapes between spheres and saddles. The saddle line is normal to the astigmatism line and hence evolution under uniform normal motion can predict saddle shapes only due to a stagnation process, where V = 0.

View Article Online
DOI: 10.1039/C7SM02409F

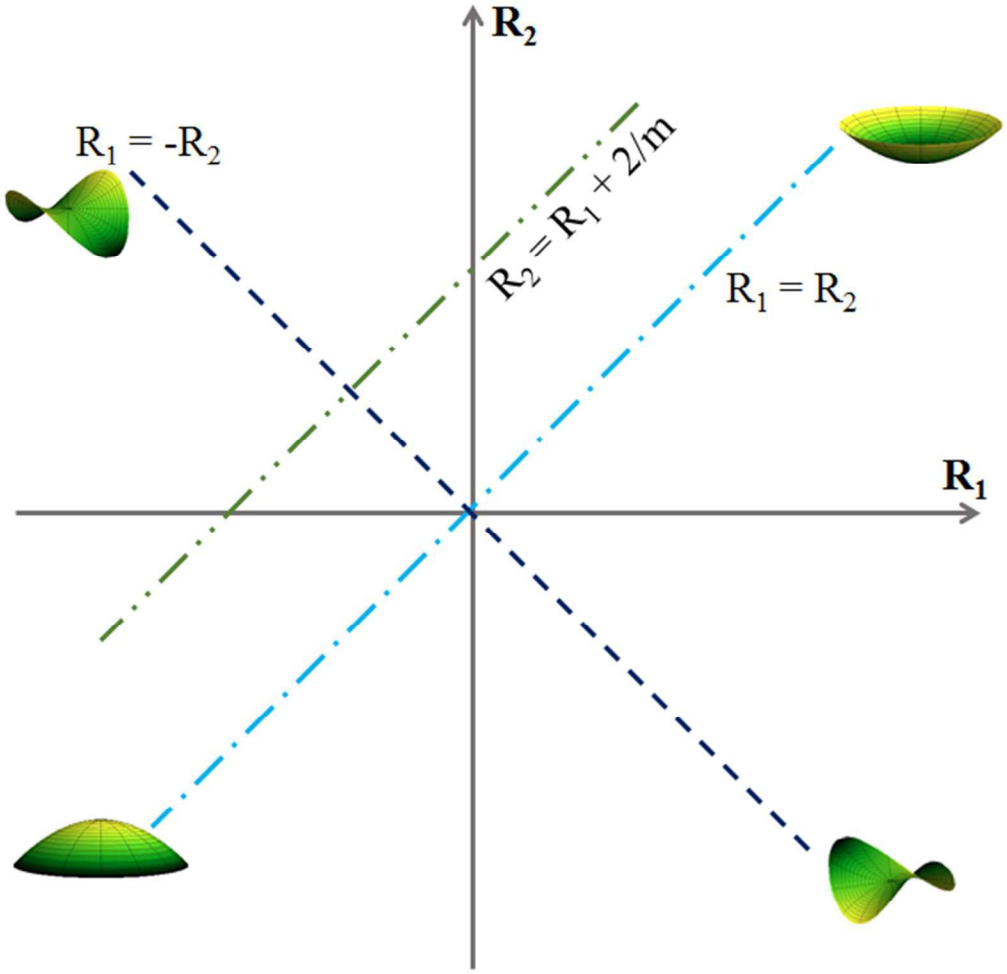

View Article Online
DOI: 10.1039/C7SM02409F

Figure 6. Evolution under normal uniform motion (V=const.; eqn. (13)) showing the sphere (light blue dot-dash line), saddle (dark blue dash line) and astigmatic trajectories (green double dot-dash line) found from eqn.(14). Evolution is along the positive slope lines, with m defining the ratio between K and D. Since the astigmatic trajectories are normal to the saddle line, this means that saddles can only form through freezing (V=0).

Figure 7 show the curvature trajectories in the HD plane obtained by integrating eqns. (12 a-b), which were validated with the analytical solutions provided in Appendix B. The diagonals correspond to the cylinder, the parabolas to saddles and the horizontal to spheres. The origin corresponds the flat surface. Cylinder and sphere expansion start at the flat origin. In agreement with the astigmatism equation (14), saddles can only form saddle ruts and saddle ridges when V = 0. The particular saddle is defined at the intersection of the saddle line (vertical axis) and the astigmatic line $K = -mD$ (see Appendix C) yielding $D = |m|$. Thus on the vertical H=0 line we find saddles whose Gaussian curvature is $-m^2$.

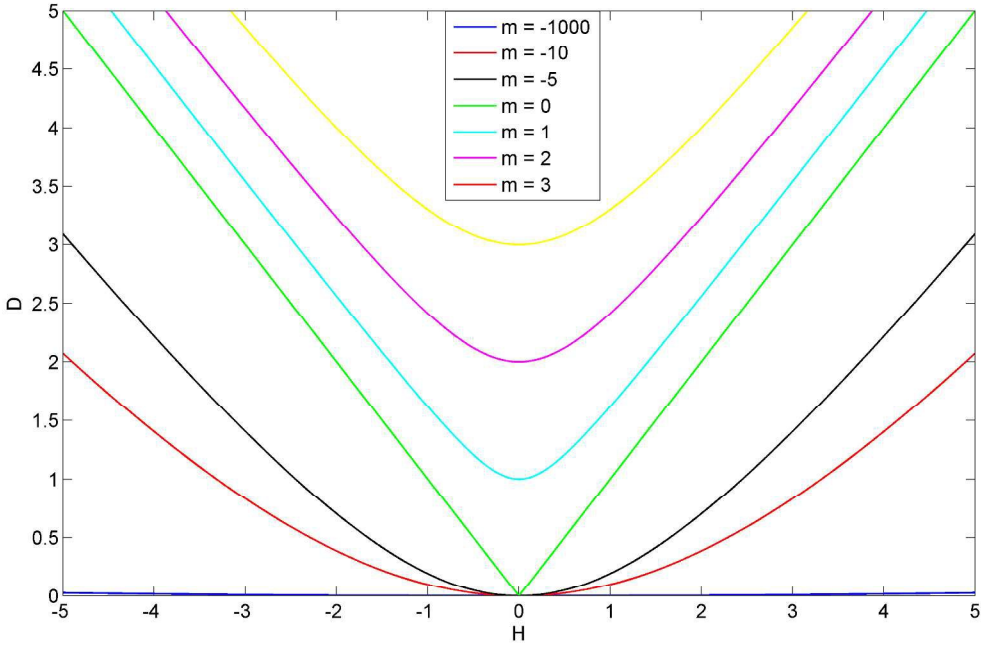

Figure 7. Deviatoric curvature D as a function of mean curvature H. Sphere and cylinder trajectories pass through the flat surface origin. Saddles can be formed from saddle ridges and saddle ruts through stagnation (normal velocity V=0). The trajectories obey the astigmatism eqn. (13).

View Article Online
DOI: 10.1039/C7SM02409F

(ii) Shape Evolution

Using the transformation matrix in eqn. (7), the SC evolution is:

$$\frac{dC}{dt} = \mathrm{V}\left(\sin\left(\frac{S\pi}{2}\right) + c\cos\left(\frac{S\pi}{2}\right)\sin\left(S\pi\right)\right)C^2$$
$$\frac{dS}{dt} = V\left(\cos\left(\frac{S\pi}{2}\right) - \sin\left(\frac{S\pi}{2}\right)\sin\left(S\pi\right)\right)\frac{2C}{\pi} \qquad \text{(15 a-b)}$$

For $\left(V \neq 0\right)$, the only steady state is the flat surface. The shape invariant evolution is

$$\cos\left(\frac{S\pi}{2}\right) - \sin\left(\frac{S\pi}{2}\right)\sin\left(S\pi\right) = 0 \qquad (16)$$

corresponding to spherical ($S = \pm 1$) and cylindrical ($S = \pm 1/2$) patches.

Next, we describe the astigmatic flow in the SC morphological space. Using the transformation matrix and eqn. (13) the shape-curvedness evolution is:

$$\cos\left(\frac{S\pi}{2}\right) = \frac{m \pm \sqrt{m^2 + 8C^2}}{4C} \qquad (17)$$

shown in Figure 8. As per eqn. (17), the only constant shape evolutions are the sphere ($S = \pm 1, m \to \infty$) and the cylinder ($S = \pm 1/2, m = 0$). At C = 0 the shape is undefined. Growth (dissolution) is downwards (upwards). Dome shapes grow towards spherical shapes and saddle ridges towards perfect saddles.

View Article Online
DOI: 10.1039/C7SM02409F

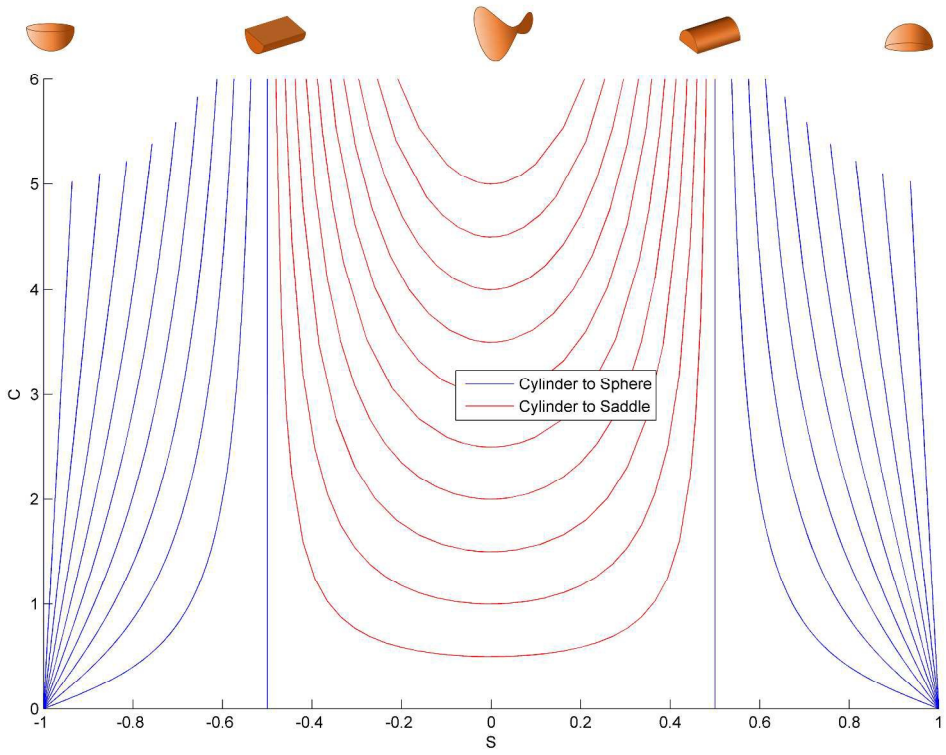

Figure 8. Trajectories in morphological space. Curvedness as a function of shape for evolution under uniform normal motion. Growth (shrinkage) is downwards (upwards).

The geometric evolution is characterized by the change of curvedness with respect to changes in shape:

$$\frac{dC}{dS} = \frac{-m\frac{\pi}{2}\sin\left(\frac{S\pi}{2}\right)\cos\left(S\pi\right) - m\cos\left(\frac{S\pi}{2}\right)\sin\left(S\pi\right)}{\cos^2\left(S\pi\right)} \tag{18}$$

which diverges for cylinders and spheres and vanishes for saddles. Under growth or decreasing C, trajectories that start close to spheres or cylinders remain nearly shape invariant. On the other hand, for starting shape between -1/2<S<1/2, changes in shape are stronger and saddles are realizable.

(iii) Frozen Shapes

View Article Online
DOI: 10.1039/C7SM02409F

As discussed in Section 2.2, under stagnation conditions (V = 0) driven by thermodynamics and geometry (eqn.(11), we find the two necessary conditions that completely specify the frozen shapes:

$$C\sin\left(\frac{S\pi}{2}\right)=\Lambda,\tan\left(S\pi\right)=\frac{2\Lambda}{m} \tag{19}$$

where the constant Λ is defined in Section 2.1. Conditions for characteristic frozen shapes found from eqn.(19) are:

(i) saddles: $S=0, C=m, \Lambda=0$

(ii) cylinders: $S=\pm 1/2, C=2\Lambda/\sqrt{2}$

(iii) spheres: $S=\pm 1, C=\Lambda$

For flow under mean curvature, $V=-2\left(\gamma+\mathbf{I}_s:\partial^2\gamma/\partial\mathbf{k}^2\right)H/\beta=bC\sin\left(S\pi/2\right)/\beta$,

stagnation arises when $\Lambda=0$ and only static saddles can form. For the general case, for a given Λ, we find that the curvedness of the frozen shapes increases with S. The stagnation flow trajectories (V=0) are superposed in the CS plane with the astigmatic trajectories (replotted from Figure 8) in figure 9. For a given (m, Λ) the crossing between the full line and the freezing line gives the selected shape. For (m=0, $\Lambda=\sqrt{2}/2$) the selected frozen shape is a cylinder of curvedness C=1.

View Article Online
DOI: 10.1039/C7SM02409F

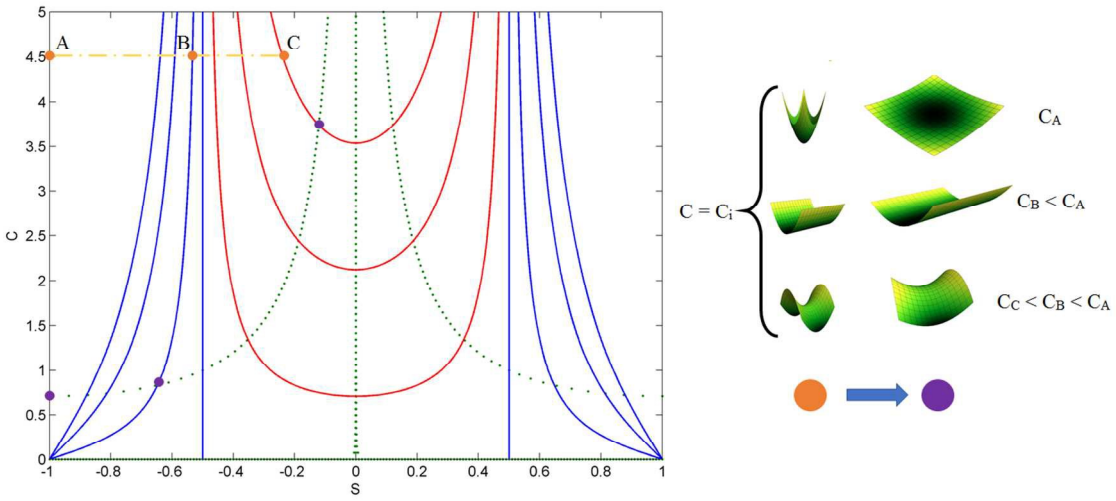

Figure 9. (Left panel) Trajectory phase-plane with the trajectories from Figure 8 superposed with stagnation lines (green curves) which are solutions to eqns.(19). For a given (m,Λ) the crossing between the full line and the freezing line gives the selected shape. For (m=0, $\Lambda = \sqrt{2}/2$) the selected frozen shape is a cylinder of curvedness C=1.(right panel) Starting with a spherical (A), trough (B), and saddle rut (C) patches (orange dots) evolution with freezing leads the spherical, trough and saddle rut with increasing curvedness (purple dots) , but saddle-like figure freeze at higher curvature and spheres at lower curvatures.

These results show that if one starts with a uniform distribution of shapes between spheres and saddles under decreasing C conditions (growth towards flat planes), potential static spherical shapes will be closer to flat surfaces than cylinders and saddle ridges. Such scenario is depicted on the left panel of Fig. 9 where the orange horizontal line represents the uniform distribution with the same initial curvedness, whose trajectories lead to different final curvedness under decreasing C conditions, where the frozen state is represented by the purple dots. It should be noted the frozen saddles have higher curvedness than the frozen spheres. Under increasing C conditions, the same effect is predicted.

4. Conclusions

View Article Online
DOI: 10.1039/C7SM02409F

In this paper we introduced a previously presented approach [8] to decouple shape from curvedness, to analyze basic equations of interfacial transport phenomena. The objective is to disentangle the unique effects from shape from curvedness as these are fundamental to biological morphology, interfacial phenomena, and phase transitions in soft and hard materials. We demonstrated the usefulness of shape methodology by applying it to the surfactant packing parameter case and to the normal motion of surfaces for diffusionless phase transitions. Using a simple surface kinematics, that is uniform normal motion, we derived the shape-curvedness equations. We compared the results of this kinematics by finding analytical solutions for trajectories in curvature HD space and in morphological SC space. We found that uniform normal motion leads to "astigmatic" trajectories in which the radii of curvature are linearly dependent at all times. On the morphological space, we showed that the astigmatic trajectories can be clearly classified into two modes; (i) constant shape evolution, and (ii) variable shape-variable curvedness. The shapes between spheres and cylinders follow approximately the former mode for large curvedness and then transition at smaller curvedness into the latter mode. Shapes between cylinder and saddles only follow the second mode. Under geometry-driven stagnation (zero normal velocity) shapes can be frozen. Under given thermodynamic conditions growing spheres freeze later than cylindrical which in turn freeze later than saddle-like patches. The results provide a complementary view on how to describe and control shape evolution in surfaces and interfaces of great relevance to biological, colloidal and interfacial science.

References

1. Hiroaki Masuda, Ko Higashitani, Hideto Yoshida, Powder Technology Handbook, Third Edition

View Article Online
DOI: 10.1039/C7SM02409F

2. Nielsen, Lauge Fuglsang. *Composite materials: properties as influenced by phase geometry*. Springer Science & Business Media, 2005.
3. Adams, J. M. "Particle size and shape effects in materials science: examples from polymer and paper systems." *Clay Minerals* 28.4 (1993): 509-530.
4. D. A. Edwards, H. Brenner, and D.T. Wasan, Interfacial Transport Processes and Rheology, Butterworth-Heinemann, Stonheam, 1991.
5. S. Hyde, S. Andersson, K. Larsson, Z. Blum, T Landh, S. Lidin, B.W. Ninham, The Language of Shape, Elsevier, Amsterdam, 1997.
6. Koenderink, Jan J., and Andrea J. Van Doorn. "Surface shape and curvature scales." *Image and vision computing* 10.8 (1992): 557-564.
7. Dryden, Ian L., and Kanti V. Mardia. *Statistical Shape Analysis: With Applications in R*. John Wiley & Sons, 2016.
8. Koenderink, Jan, Andrea van Doorn, and Johan Wagemans. "Local Solid Shape." *i-Perception* 6.5 (2015): 2041669515604063.
9. Davies, Jamie. *Mechanisms of morphogenesis*. Academic Press, 2013.
10. Chang, Fred, and Kerwyn Casey Huang. "How and why cells grow as rods." *BMC biology* 12.1 (2014): 54.
11. Gibbs, J. W., K. Aditya Mohan, E. B. Gulsoy, A. J. Shahani, X. Xiao, C. A. Bouman, M. De Graef, and P. W. Voorhees. "The three-dimensional morphology of growing dendrites." *Scientific reports* 5 (2015): 11824.
12.Drew, Donald A. "Evolution of geometric statistics." *SIAM Journal on Applied Mathematics* 50.3 (1990): 649-666.
13.Glicksman, Martin Eden. *Principles of solidification: an introduction to modern casting and crystal growth concepts*. Springer Science & Business Media, 2010.
14.J.D. Eliassen, PhD Thesis (University of Minnesota, Minnesota, 1963).
15. Daudin, R., S. Terzi, P. Lhuissier, J. Tamayo, M. Scheel, N. Hari Babu, D. G. Eskin, and L. Salvo. "Particle-induced morphological modification of Al alloy equiaxed dendrites revealed by sub-second in situ microtomography." *Acta Materialia* 125 (2017): 303-310.
16. B. Wincure and A.D. Rey, "Nano Scale Analysis of Defect Shedding from Liquid Crystal Interfaces", *Nano Letters*, **76**, 1474-1479, 2007; Wincure, Benjamin, and Alejandro D. Rey. "Computational modelling of nematic phase ordering by film and droplet growth over heterogeneous substrates." *Liquid Crystals* 34.12 (2007): 1397-1413.
17. B. Wincure and A.D. Rey, "Growth regimes in Phase Ordering transformation", *Discrete and Continuous Dynamical Systems,* Series B, vol. **8** 3, 623-648, 2007; Wincure, Benjamin, and Alejandro D. Rey. "Interfacial nematodynamics of heterogeneous curved isotropic-nematic moving fronts." *The Journal of chemical physics* 124.24 (2006): 244902.
18. B. Wincure and A.D. Rey, "Growth and structure of nematic spherulites under shallow thermal quenches", *Continuous Mechanics and Thermodynamics*, **19**, 37-47, 2007.
19. Abukhdeir N. M., Soulé E. R., A.D. Rey, "Non-Isothermal Model for Nematic Spherulite Growth", *Langmuir*, **24**23, 13605-13613, 2008.
20. Abukhdeir N. M., Soulé E. R., A.D. Rey, "Shape-dynamic growth, structure, and elasticity of homogeneously oriented spherulites in an isotropic/smectic-a mesophase transition", *Liquid Crystals,* **36**10-11, 1125-1137, 2009; Gurevich, S., Provatas, N. and Rey, A., 2017. Nanoscale interfacial defect shedding in a growing nematic droplet. *Physical Review E*, *96*(2), p.022707; Gurevich, Sebastian, et al. "Self-assembly via branching morphologies in nematic liquid-crystal nanocomposites." *Physical Review E* 90.2 (2014): 020501.
21. Fultz, Brent. *Phase transitions in materials*. Cambridge University Press, 2014.
22. P.A. Kralchevsky., K. Nagayama, Particles at Fluids Interfaces and Membranes , Elsevier: Amsterdam, **2001**.
23. Ljunggren,S., Eriksson, J.C., Kralchevsky, P. *Journal of Colloid and Interface* Science **1997**, 191, 424.

View Article Online
DOI: 10.1039/C7SM02409F

24. Kralchevsky, P.A., Eriksson, J.C.,Ljunggren,S.*Advances in Colloids and Interface Science***1994**, 48, 19.
25. Eriksson, J.C., Ljunggren,S. In : *Surface and Interfacial Tension*, S. Hartland editor, Surfactant Science Series 119, Marcel Dekker: New York, 547-614 **2004** .
26. Zund, J. D. "Tensorial methods in classical differential geometry-II: basic surface tensors." *Tensor* 47.1 (1988): 83-92.
27. A.D. Rey, "Linear Viscoelastic Model for Bending and Torsional Modes in Fluid Membranes", *Rheologica Acta,* **47**, 861-871, 2008.
28. A.D. Rey, "Polar Fluid Model of Viscoelastic Membranes and Interfaces", *Journal of Colloid and Interface Science*, **304**1, 226-238, 2006.
29. O. A. Gutierrez, E. E. Herrera-Valencia and A.D. Rey, JCIS-16-2363R1, "Generalized Boussinesq-Scriven Surface Fluid Model with Curvature Dissipation for Liquid Surfaces and Membranes", *Journal of Colloid and Interface Science,* 2 Mar 2017.
30. Pavlov, Maxim V., and Sergej A. Zykov. "Lagrangian and Hamiltonian structures for the constant astigmatism equation." *Journal of Physics A: Mathematical and Theoretical* 46.39 (2013): 395203.
31. Hlaváč, Adam, and Michal Marvan. "Another integrable case in two-dimensional plasticity." *Journal of Physics A: Mathematical and Theoretical* 46.4 (2013): 045203.

Acknowledgements

This research was supported by a grant from the Natural Sciences and Engineering Council of Canada. ADR is thankful to McGill University for financial support through the James McGill Professorship appointment.

View Article Online
DOI: 10.1039/C7SM02409F

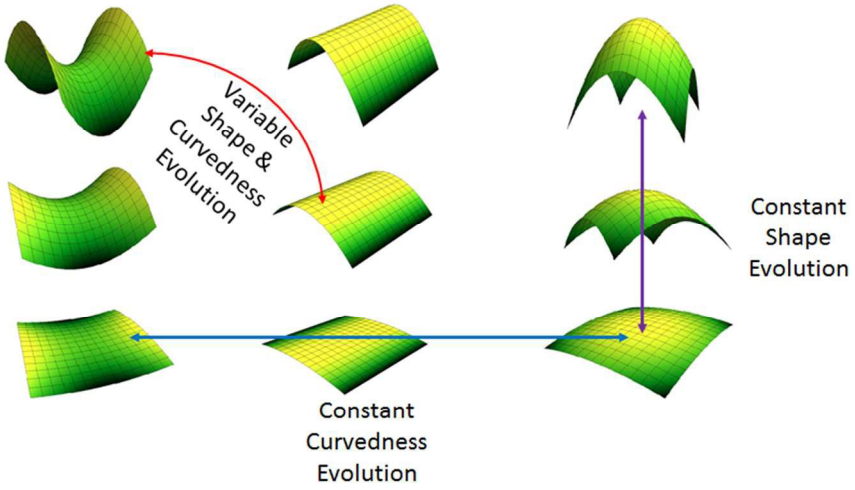

246x138mm (96 x 96 DPI)